LASER INTERFEROMETER GRAVITATIONAL WAVE OBSERVATORY

LIGO Laboratory / LIGO Scientific Collaboration

LIGO-T060224-v7 *Advanced LIGO* June 9, 2011

TCS Actuator Noise Coupling

Phil Willems

Distribution of this document:
LIGO Scientific Collaboration

This is an internal working note
of the LIGO Laboratory.

California Institute of Technology
LIGO Project – MS 18-34
1200 E. California Blvd.
Pasadena, CA 91125
Phone (626) 395-2129
Fax (626) 304-9834
E-mail: info@ligo.caltech.edu

Massachusetts Institute of Technology
LIGO Project – NW22-295
185 Albany St
Cambridge, MA 02139
Phone (617) 253-4824
Fax (617) 253-7014
E-mail: info@ligo.mit.edu

LIGO Hanford Observatory
P.O. Box 1970
Mail Stop S9-02
Richland WA 99352
Phone 509-372-8106
Fax 509-372-8137

LIGO Livingston Observatory
P.O. Box 940
Livingston, LA 70754
Phone 225-686-3100
Fax 225-686-7189

http://www.ligo.caltech.edu/

1 Introduction

This document provides a detailed estimate of the coupling of TCS actuator power fluctuations into interferometer noise. It follows the analysis Stefan Ballmer used in his thesis, but with extension to the noise requirements for compensation plates, ring heaters acting on the barrel of test masses, and transmissive flexure noise.

2 Corrections to the previous versions of this document

2.1 Corrections to version 1

The formula for the heat diffusion length was incorrect in the previous version of this document, and has been changed.

This document includes an analysis of test mass flexure noise that was left 'TBD' in the previous version.

The required noise level has been revised from $5x10^{-22}$m/√Hz at 100 Hz, to $1x10^{-22}$m/√Hz at 250 Hz. The actual aLIGO technical displacement noise spectrum is rather complex but this value at that frequency is the most stringent for the 1/f spectrum of the noise coupling and so provides a conservative estimate of noise requirements.

2.2 Corrections to version 3

The calculations have been redone to reflect the new CP thickness of 10 cm.

The noise requirements are now given as detailed spectra rather than specified at the most stringent frequency.

Jitter noise coupling is now included in the requirements.

The overall exposition has been revised for better clarity.

2.3 Corrections to version 4

The angle of incidence of the CO_2 laser projector beam on the CP in the folded IFO has been updated from ~35° to 44°.

2.4 Corrections to version 5

A new section considering electrostatic forces on the test mass from the ring heater has been added.

2.5 Corrections to version 6

The section considering electrostatic forces on the test mass from the ring heater has been revised to consider transverse forces and torques.

3 Requirements

The effective displacement noise injected into the arm cavity by TCS must be less than the spectrum in Figure 1.

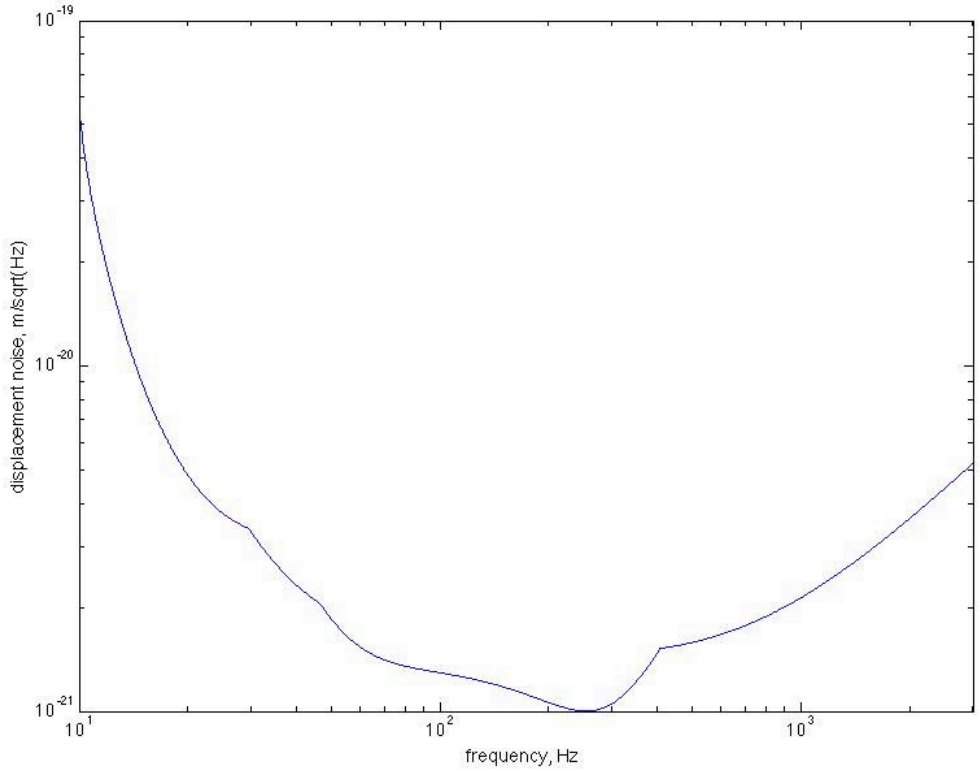

Figure 1: Maximum allowable technical displacement noise of the aLIGO test mass.

This spectrum is the limit to the motion of the test mass HR surface, which would inject noise directly into the highly sensitive arm cavity. The substrate of the test mass (TM) and the compensation plate (CP) reside in the recycling cavity, and so their noise limit is scaled from this spectrum by a factor $2F/\pi$, where F is the arm cavity finesse.

4 Summary of coupling mechanisms

Later we will give a full description of the functional dependence of the TCS noise couplings. Here, we briefly describe the physical mechanisms that are responsible.

1) The thermorefractive effect: fluctuations in the optic temperature change its index of refraction. This is the dominant effect in the compensation plate.
2) The thermoelastic effect: fluctuations in the optic temperature cause it to expand. This is less than $1/10^{th}$ as large as the thermorefractive effect.
3) Flexure: thermoelastic expansion in one part of the optic causes the entire optic to change its shape. This is the dominant effect in the test mass.
4) The elasto-optic effect: strain fields associated with flexure change the index of refraction of the optic. This effect is negligible compared to the others here.

5) Radiation pressure: variations in the light power change the force on the optic. This has two consequences. The force will compress the optic, and the optic will recoil from the force. The compression causes significant coupling, while the recoil does not.
6) Dependence of optic infrared absorption with incident angle. This converts incident beam jitter into absorbed power fluctuations.
7) Electrostatic forces on the test mass by the ring heater.

5 Model

We begin with Stefan Ballmer's derivation of the detector noise due to TCS amplitude fluctuations.[1] His derivation was for TCS projected onto the face of the ITM, while here we are concerned with TCS projected onto the face of the CP or on the barrel of the TM, but the basic principles still apply. Numerical values for all material and interferometer parameters are given in Section 11.

Assume a Cartesian coordinate system x,y,z, where the optical axis is along z. Further assume a heating pattern $p(x,y)$ on the face of an optic, and that the heat power oscillates in time with frequency f, inducing a fluctuating temperature in the optic $T(x,y,z)$. Within the aLIGO detection frequency band, the diffusion depth $t \approx \sqrt{D_{th}/(2\pi f)} \approx 35$ microns into the optic is much smaller than the scale of variation of $p(x,y)$, and so the heat flow in this thin layer is effectively one-dimensional. The surface energy density $E(x,y)$ in the layer is given by

$$E(x,y) = \rho C_v \int T(x,y,z)dz .$$

Here, ρ and C_v are the density and heat capacity of fused silica. The energy density is related to the heating by $\dot{E}(x,y) = p(x,y)$, so we have

$$p(x,y) = 2\pi i f \rho C_v \int T(x,y,z)dz .$$

Notice that for fixed $p(x,y)$ the integral over T is inversely proportional to the fluctuation frequency f. Because of this, all the noise coupling mechanisms considered here are also inversely proportional to f. The heated surface layer will thermoelastically expand by an amount $(1+\eta)\alpha \int T(x,y,z)dz$, thus changing the CP optical thickness, and the optical length of the recycling cavity will undergo a thermoelastic change Δz_{TE} of

$$\Delta z_{TE}(x,y) = (n-1)(1+\eta)\alpha \int T(x,y,z)dz .$$

Here, n is the index of refraction of fused silica, and η and α are its Poisson ratio and thermal expansion coefficient.

The refractive index of the thin surface layer will also change with temperature. This causes an additional thermorefractive change Δz_{TR} in the optical path

[1] Stefan Ballmer, Ph.D. thesis

$$\Delta z_{TR}(x,y) = \frac{dn}{dT}\int T(x,y,z)dz$$

which is added to the thermoelastic path change. Note that we do not consider the thermoelastic or thermorefractive properties of the CP AR coating to differ from those of fused silica. We have no data for the CP AR coating to use in this model.

There are two other physical mechanisms that convert TCS fluctuations into detector noise. These are test mass flexure (Δz_F), and elasto-optic modulation caused by test mass flexure (Δz_{EO}). These are not so straightforwardly derived as the thermoelastic and thermorefractive couplings described above, but can be easily calculated using a finite element model. Section 9 describes how to do this. Putting these all together we get

$$\Delta z(x,y) = \Delta z_F(x,y) + \Delta z_{EO}(x,y) + \left[(n-1)(1+\eta)\alpha + \frac{dn}{dT}\right]\frac{p(x,y)}{2\pi i f \rho C_v}.$$

Finally, we must weight this effective displacement profile over the interferometer beam profile

$$\frac{2}{\pi w^2}\exp\left(-2\frac{x^2+y^2}{w^2}\right).$$

Radiation pressure does not introduce significant noise from TCS. The interferometer is not strongly sensitive to the CP displacement, either along the beam axis or transverse to it, but rather to changes in the CP's optical thickness.

6 Compensation plate noise couplings

The following heating pattern on the compensation plate was found by modeling to provide nearly ideal compensation to an ITM that absorbs the nominal 0.5 ppm of the full arm cavity power and is curvature corrected by its ring heater:

$$p(x,y) = 160\exp\left(-2\frac{(r-.1m)^2}{(.106m)^2}\right)\frac{W}{m^2}$$

where $r^2 = x^2 + y^2$. The scatter out of the recycling cavity mode for this profile was found to be 0.13%. A superior 'ideal' heating profile is likely to exist, but our profile is quite good, has a very simple functional form, and should have nearly identical noise coupling to the ideal profile. The total power delivered to the CP by this pattern is $11W$.

The overlap integral of this heating profile with the IFO beam can be easily calculated and is $73.7W/m^2$. The combined thermoelastic and thermorefractive coupling is then

$$\Delta z_{TE+TR} = \left[(n-1)(1+\eta)\alpha + \frac{dn}{dT}\right]\frac{73.7W/m^2}{2\pi i f \rho C_v} RIN$$

If we apply this formula to the noise spectrum for the compensation plate we get the following requirement on the TCS projector amplitude noise:

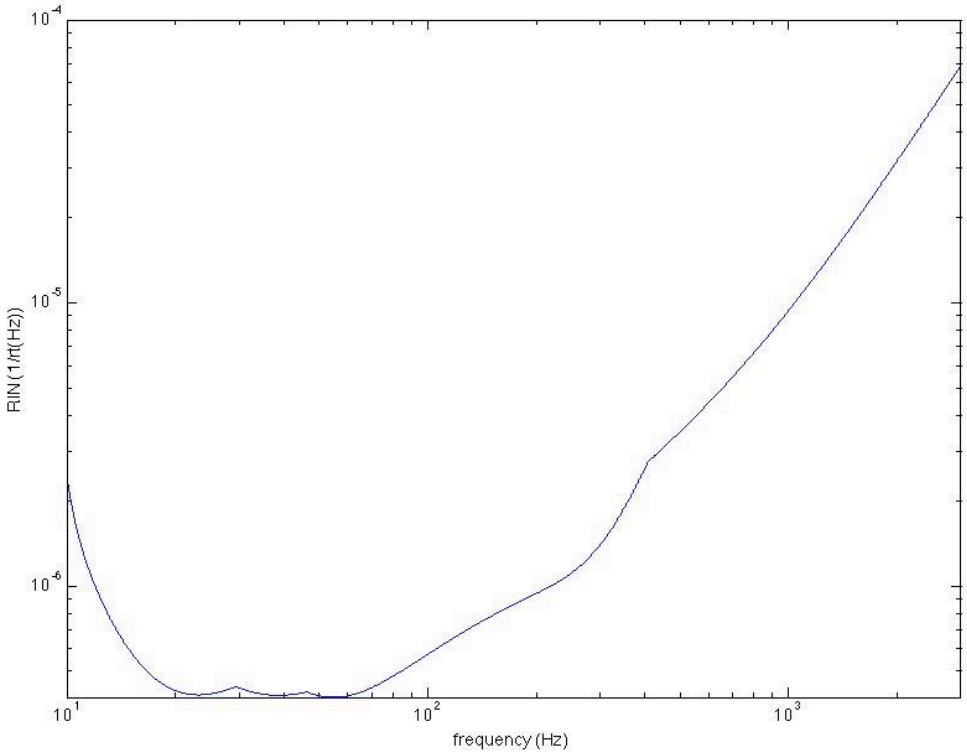

Figure 2: Amplitude noise requirement for the TCS projector.

The combined direct thermoelastic and thermorefractive coupling of TCS noise power to CP optical path is $6.41\times10^{-12} m/W$ at $10 Hz$. We will now show that all other noise couplings in the CP are negligible in comparison.

We applied the stress field induced by a brief fluctuation of the heating profile $p(x,y)$ to a model of the compensation plate in COMSOL, in order to evaluate the flexure and elasto-optic contributions to the noise coupling. As explained in the appendix, the noise is proportional to the difference of the displacements of the front and rear CP surfaces. This profile is plotted in Figure 3.

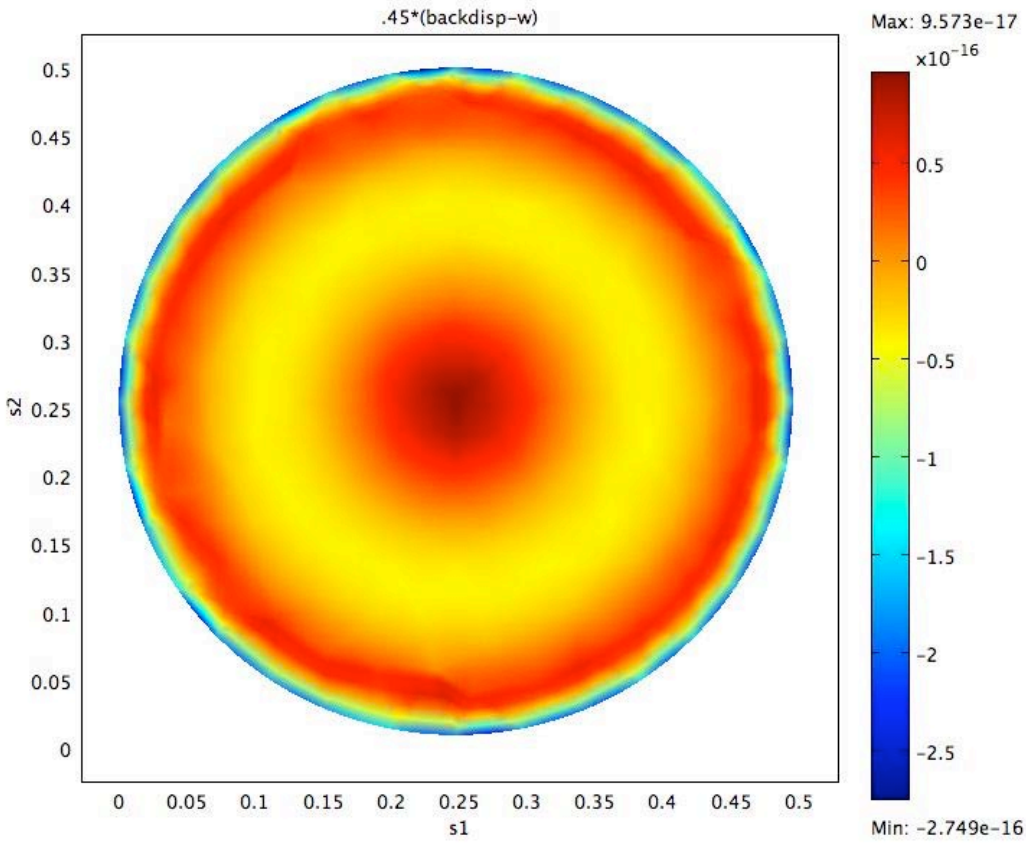

Figure 3: profile of thickness change in the CP.

We must scale this profile by the modeled fluctuation level to convert this profile into an injected noise level. In the COMSOL model, we used the temperature profile that would result from a RIN of 5.11×10^{-3} at $10\,Hz$ to get the figure above. The noise coupling is of order $2\times10^{-15}\,m/W$ and so is negligible compared to the direct thermoelastic and thermorefractive couplings.

The elasto-optic profile through the CP resulting from this same fluctuation is shown in Figure 4. The scale of the optical path is of order $1\times10^{-16}\,m/W$ and so this coupling too is negligible compared to the direct thermoelastic and thermorefractive couplings.

Fluctuations in radiation pressure from the $11W$ projected beam lead to a CP recoil at $10\,Hz$ of $4.6\times10^{-13}\,m/W$. While this appears not to be very small compared to the direct thermoelastic and thermorefractive noise couplings, it is in fact negligible. One reason is that the recoil falls as $1/f^2$ (by the simple formula $F=ma=m\ddot{x}=-m\omega^2x$), and so becomes insignificant very rapidly at higher frequencies relative to other couplings that fall as $1/f$. The other reason is that the interferometer is not very sensitive to displacement of the CP, but rather to changes in its optical depth.

Fluctuations in radiation pressure do change the optical depth of the CP, by compressing it. This compression is independent of frequency. It can be roughly estimated by

$$\frac{l}{YAc}\cdot RIN = 5.1\times10^{-20}\,m/W$$

where l is the CP thickness, A its area, and Y its Young's modulus. Even at $1000\,Hz$ this is much less than the direct thermoelastic and thermorefractive noise and can be ignored.

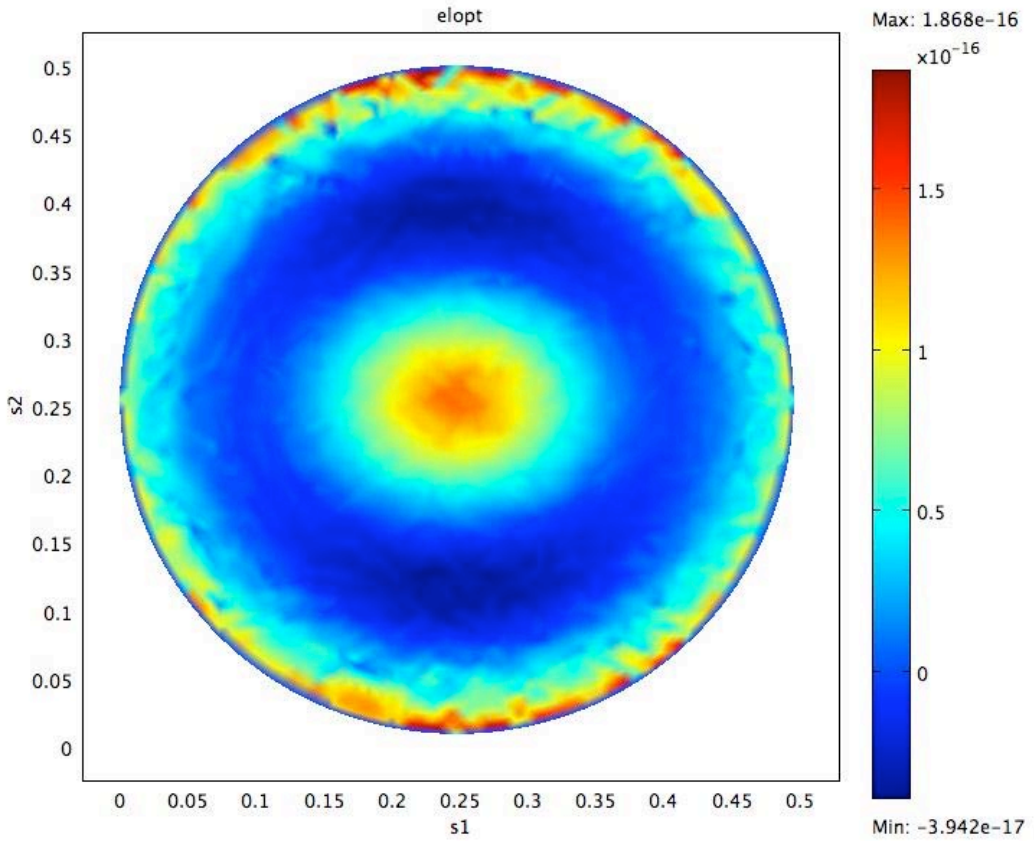

Figure 4: Elasto-optic noise profile in the CP.

7 Test mass noise couplings

TCS acts upon the test masses: directly, through the ring heaters, and indirectly upon the ITM via heating by the CP. The time scale for the CP to heat the ITM is hours and we need not consider it as a possible noise coupling. The ring heater power fluctuations couple immediately to the test mass and cannot be trivially dismissed.

The formulae in the appendix were input to a 2D model in COMSOL[2] and generated the deformation plot given below in Figure 5. Comparison of the motion of the ITM HR surface to the motion of the center of mass gives a transfer function of

$$\left\langle \Delta z_{flexure} \right\rangle = -9.47 \times 10^{-15}\, m \cdot \left(\frac{10\,Hz}{f} \right) \cdot \left(\frac{P}{1W} \right) \cdot RIN$$

[2] This 2D model did not include the flats on the sides of the TM.

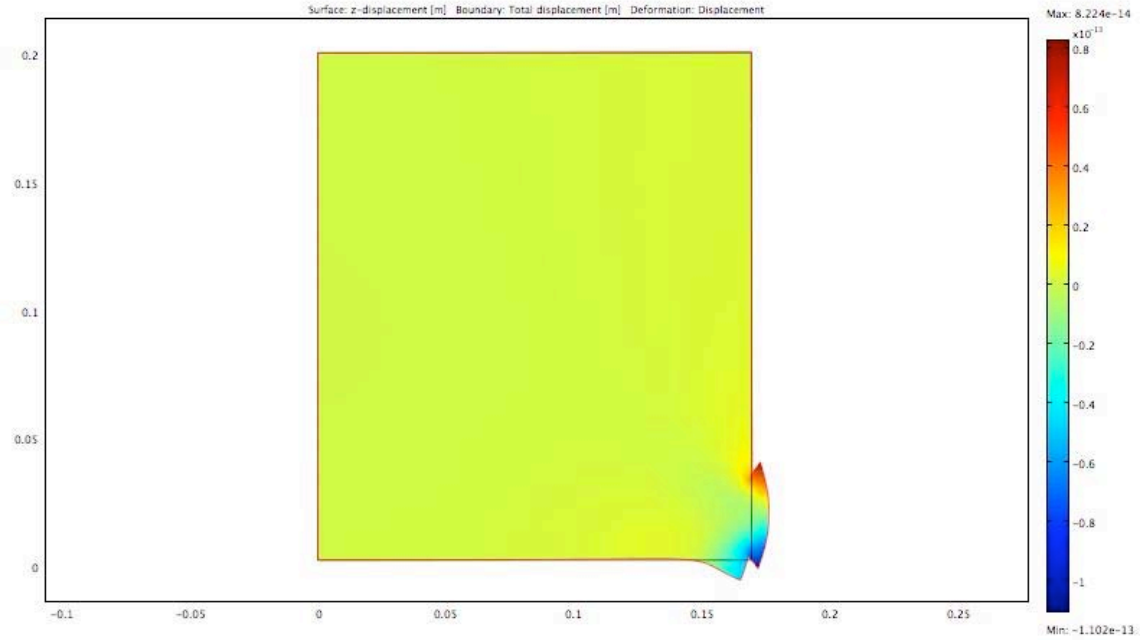

Figure 5: deformation of the TM due a fluctuation in the ring heater power. The 2D plot extends from zero radius to the TM outer radius of 0.17m.

In LIGO document T1000093-v1 it is shown that the required power stability for the ring heater supply to meet the aLIGO noise requirement is trivially met, for the case of a Watlow-style ring heater where a metal sheath encloses the resistive element.

Direct thermoelastic and thermorefractive coupling of ring heater noise to the optical path in the substrate of the ITM may be ignored; the thermal fluctuations penetrate only about 35 microns inward from the barrel. The elastooptic phase profile from the flexure of the test mass does penetrate the whole ITM substrate. This profile is shown in Figure 6. The effective displacement coupling is

$$\langle \Delta z_{EO} \rangle \approx 1 \times 10^{-14}\, m \cdot \left(\frac{10\,Hz}{f} \right) \cdot \left(\frac{P}{1W} \right) \cdot RIN$$

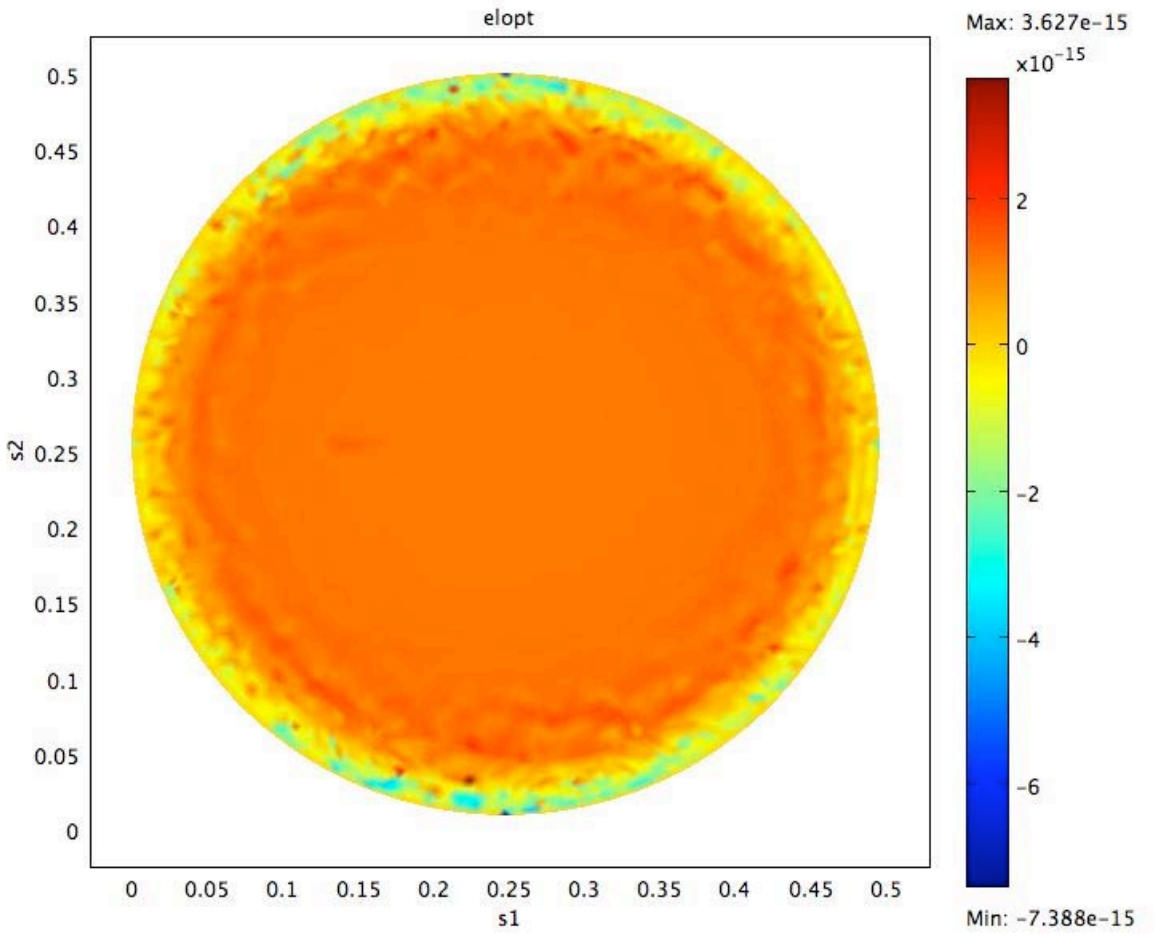

Figure 6: Elasto-optic profile in TM due to ring heater power fluctuation.

This is about the same size as the flexure noise coupling in the TM, but since the elasto-optic noise is injected only into the recycling cavity, the requirements on it are $2F/\pi = 283$ times less stringent than for the flexure noise coupling. So, if the ring heater power noise stability is trivially met for the flexure noise, it is also trivially met for elasto-optic noise.

Electrostatic forces on the test mass due to the ring heater are derived in Section 10.4. In particular, the allowable voltage noise spectrum consistent with the ring heater design is shown in Figure 12. In LIGO document T1000249-v2, Guido Mueller calculates the current noise limit on the ring heater to be $10^{-4}\,A/\sqrt{Hz}$ due to magnetic forces on the penultimate mass by the wires carrying current to the ring heater. Assuming this current limit and multiplying by the 35Ω heater resistance yields a voltage noise limit of $3.5\times10^{-3}\,V/\sqrt{Hz}$. This is just touching the spectrum in Figure 12 at 18 Hz. Given the conservative assumptions described in Section 10.4, the voltage noise is therefore within requirements.

8 Jitter noise coupling

Jitter noise coupling is harder to estimate than amplitude noise coupling. There are additional physical coupling mechanisms to consider, and the magnitude of the coupling is sensitive to misalignment of the projected heat pattern.

'Jitter' has two related forms for the purpose of this document. 'Angular jitter' refers to changes in a beam's angle. 'Displacement jitter' refers to changes in a beam's transverse position. Angular jitter will produce displacement jitter that changes linearly with the projected beam distance. The jitter noise estimates apply only to the CO_2 laser projector beam.

8.1 CP angular absorption dependence

Angular variation of the absorbed TCS power by the CP is the easiest to describe, although as with the thermorefractive and thermoelastic effects, we do not know the variation of the AR coating infrared absorption with angle, and so we assume it to be the same as for fused silica. This function is shown in Figure 7. Note that the absorption and its angular dependence depend upon the TCS beam polarization. Indeed, by choosing the correct mixture of s- and p-polarizations the dependence of absorption on angle can be nulled. This can easily be done with a waveplate at the output of the TCS projector.

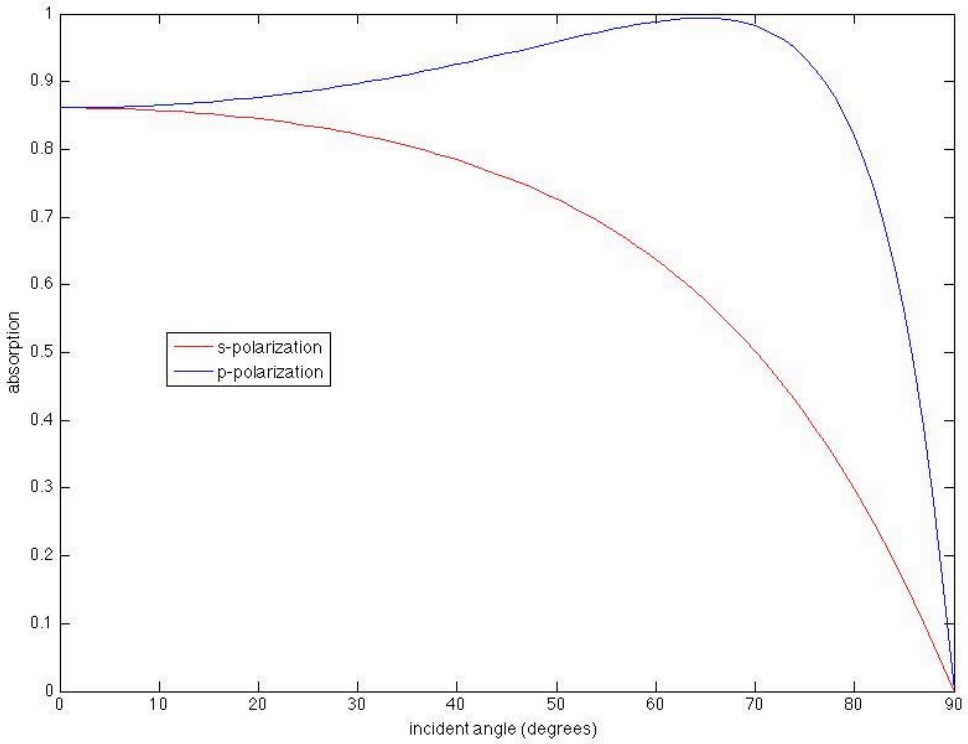

Figure 7: Absorption vs. incident angle for 10.6 micron radiation on fused silica.

Here we will assume the worst case linear polarization and calculate the resulting angular jitter noise requirement. The current aLIGO optical layout has the TCS beam incident upon the CP at ~8° in the unfolded interferometer and at 44° in the folded interferometer. The angular dependence of the absorption at 10.6 microns is $3.6\times10^{-5}/mrad$ at 8° incidence (either polarization), and $3.1\times10^{-4}/mrad$ at 35° incidence (s-polarization). We may take the maximum allowable RIN spectrum from Figure 2 and convert it into maximum allowable angular jitter noise spectra, using

the angular absorption dependence scaled by the overall absorption (~.85 for either angle) as a conversion factor. The resulting spectrum in $mrad/\sqrt{Hz}$ for 44° incidence is shown in Figure 8.

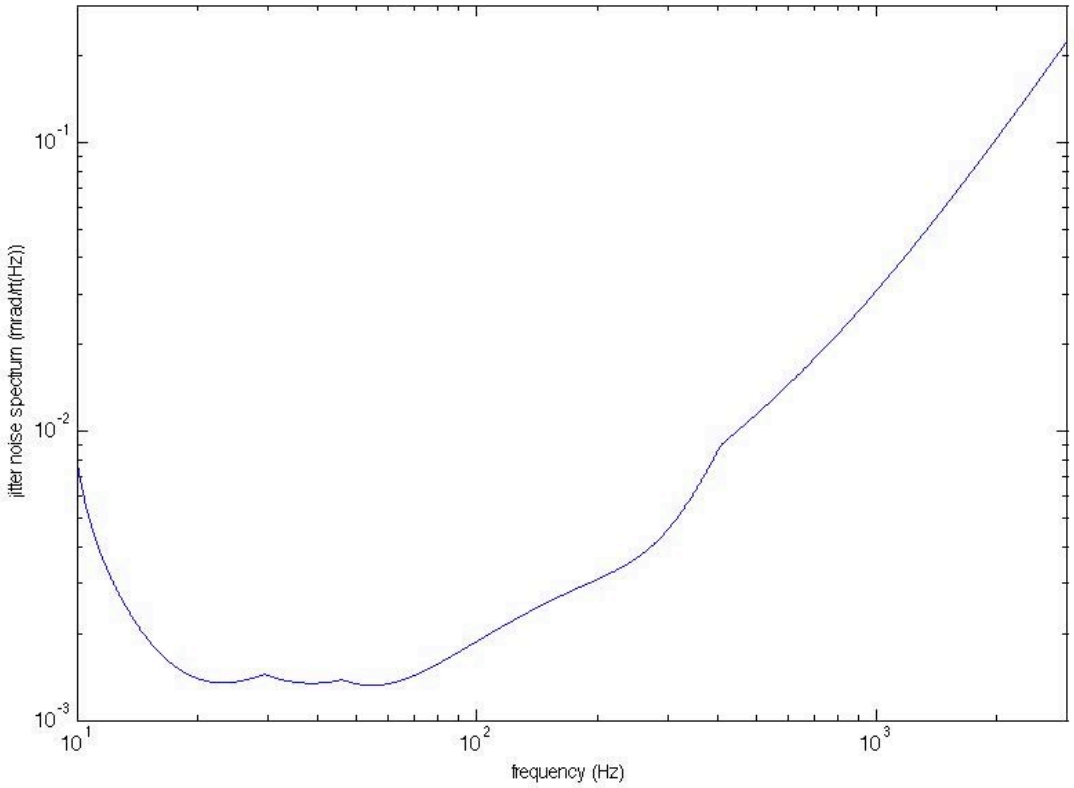

Figure 8: Allowable jitter noise spectrum due to angular dependence of CP absorption of TCS projector light.

Note that the spectrum will be 15 times less stringent for 8° incidence. Also recall that judicious choice of TCS beam polarization can reduce the sensitivity still further. This noise coupling is not strongly dependent upon the TCS beam alignment. It is possible that there is significant dependence of reflectance upon incident angle in the in-vacuum steering mirrors, which are gold-coated. We assume here that this is not the case.

8.2 Jitter fluctuations in TCS/science beam overlap

The direct thermoelastic and thermorefractive noise couplings arise because the TCS projector beam overlaps with the interferometer beam. If the TCS beam moves on the CP, the amount of overlap will change. This is another mechanism for TCS beam jitter to couple into the interferometer. The amount of coupling will depend strongly on the alignment of the TCS beam relative to the interferometer beam- if the alignment is perfectly centered, there will be no coupling to first order. The coupling will also depend on the amount and spatial distribution of stray light in the TCS projection pattern.

Here we assume that the TCS projection pattern is perfect (no stray light), but is decentered on the CP. We also assume the interferometer beam is perfectly centered on the CP. The worst case is then when the direction of the jitter is the same as the direction of the misalignment.

The variation in the overlap has the functional form

$$73.7 W/m^2 + 1.91\times 10^4 \delta^2 W/m^4,$$

where δ is the offset of the TCS beam in meters. We can now convert the direct thermoelastic and thermorefractive intensity noise spectrum into a displacement jitter noise spectrum by assuming a value for δ, and taking the derivative of the overlap function as a conversion factor. That is,

$$\Delta z_{TE+TR}\big|_{jitter} = \left[(n-1)(1+\eta)\alpha + \frac{dn}{dT}\right]\frac{3.82\times 10^4 \, W/m^4 \cdot \delta}{2\pi i f \rho C_v}\Delta x$$

where Δx is the displacement jitter amplitude (assumed small compared to the offset δ). Assuming $\delta = 1 mm$, at $10 Hz$ the coupling is $3.32\times 10^{-12}\, m/m_{jitter}$. For this offset, the displacement jitter noise spectrum that meets the technical noise curve is shown in Figure 9.

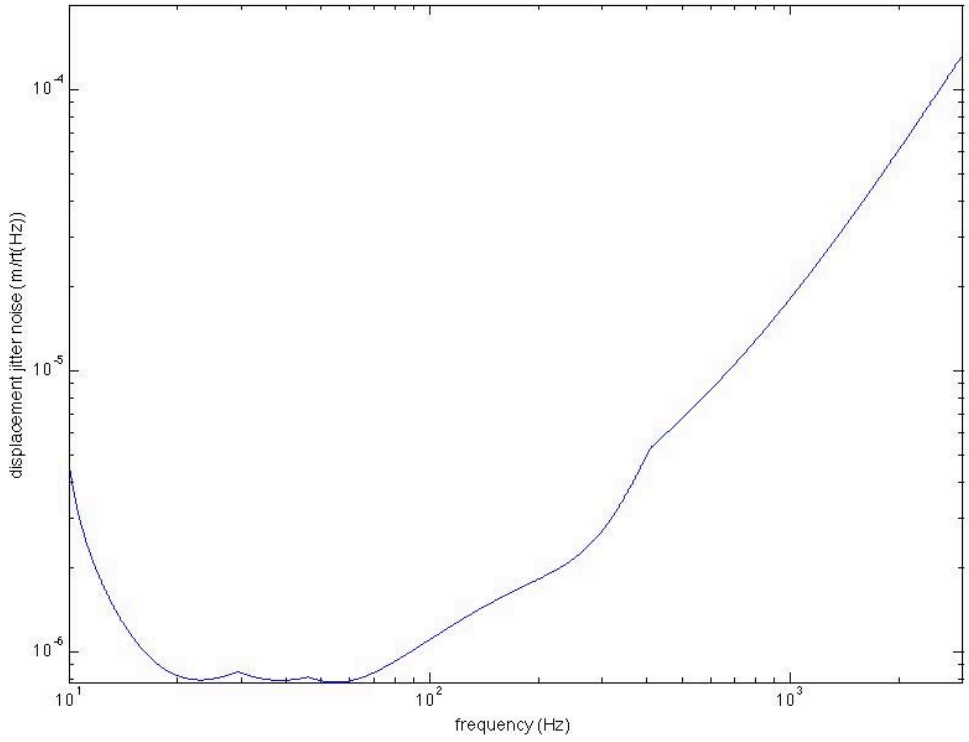

Figure 9: Jitter noise spectrum due to variations in overlap between the TCS and IFO beams.

If the offset δ is twice as large, the noise spectrum will be twice as stringent, and so on.

If there is angular jitter noise at the output of the TCS projector, it will produce displacement jitter noise at the CP in proportion to the projected beam path. For instance, at $10 Hz$ the angular jitter

will need to be less than $4 \times 10^{-7} rad/\sqrt{Hz}$ if the offset is $1mm$ and the projection path is 10 meters long. If the projection path is 50 meters long, the angular jitter will need to be 5 times smaller.

In Enhanced LIGO, this jitter noise coupling was nulled by driving the TCS table with a shaker and tweaking the alignment of TCS to the ITM until the shaker peak was no longer visible in DARM. This technique could also be used in aLIGO to the same end.

9 Conclusions and implications for TCS

The required intensity noise spectrum for the TCS projector has been analyzed, and is shown in Figure 2. The angular jitter noise spectrum is shown in Figure 8, and the displacement jitter noise spectrum in Figure 9, for the case of $1mm$ TCS projector misalignment on the CP. These are the noise requirements that must be met by the TCS projector (combined with a misalignment tolerance for the displacement jitter noise. The ring heater power noise requirement is analyzed in T1000093-v1 and the power noise requirement is given in that document.

The analyses above show a convenient way to calculate the effect of TCS fluctuations on interferometer optics by means of a constrained surface layer approximation. The advantage of this technique is that by treating the surface layer as a set of boundary forces and tractions on the substrate, it is possible to model the system in a FEM without having to mesh finely enough to sample the thin layer, or to treat the thin layer as a shell element. In addition, the constrained surface layer assumption allows these boundary forces and tractions to be simply calculated from the fluctuating heating profile.

For the case of the compensation plate, these analyses have shown that for the heating pattern we expect to use in Advanced LIGO, the flexure noise is never a significant contribution to the overall noise coupling. This is in contrast to the case of TCS on the ITMs in initial LIGO, where for annular heating the flexure noise is the dominant contribution. The difference is that for the ITM it is the motion of the HR surface relative to the center of gravity that determines the coupling, while for the CP it is the separation of the two surfaces, and the interior elasto-optic effect, that contribute, and these latter motions are much smaller.

These calculations also show that the required RIN of the CO_2 laser is at or above $4 \times 10^{-7}/\sqrt{Hz}$, which is quite practical to reach using HgCdTe detectors.

10 Appendix: flexure noise and elasto-optic noise

Flexure noise arises because the whole optic will deform under the stresses caused by thermoelastic expansion of any part of it, including a thin heated surface layer.

Because in general the HR surface of a test mass will move relative to its center of gravity as a consequence, this couples TCS intensity noise into the arm cavity (and into the recycling cavities, but this is of lesser importance). For the CP it is change of the optic's thickness under flexure that introduces noise into the recycling cavities. The stress field that flexes the optic will also make it birefringent through the elasto-optic effect.

The flexure of the optic can most easily be calculated by converting the thermal expansion of the thin heated regions into a set of stresses acting upon the optic's surface. As noted earlier, the temperature fluctuations are confined to a surface layer of order 35 microns thick. This is so thin that the rest of the mirror effectively constrains the thin layer not to expand tangentially, i.e. within

its surface. Although the mirror will deform, and the thin heated layer stretch under this deformation, the amount of stretch is so much less than it would be if the thin layer were free of the substrate, that the stretching force on the rest of the mirror can be well approximated by assuming the thin layer does not expand at all. The thin layer will also be bent due to the thermoelastic flexure of the mirror, but the forces and moments required to bend a thin layer are so small compared to those required to stretch it that they can be ignored. This is true even given the gradient of temperature across the layer's thickness, so this gradient can be ignored, and the layer approximated as having uniform temperature. The expansion of the thin layer's thickness is unconstrained.

10.1 Compensation plate flexure noise

TCS irradiates only one face of the compensation plate, so the thin heated layer causing the flexure lies in a plane. The stresses required to constrain the free thermal expansion also act in this plane.

The stress field σ required to constrain the thermal expansion of a heated body is given by

$$\sigma = Y\alpha\vec{\nabla}T$$

where Y is the Young's modulus. Let us denote $\int T(x,y,z)dz$ as $g(x,y)$. Considering only the thermal gradients in the plane of the layer, the traction required to provide this stress field is

$$\sigma_x(x,y) = Y\alpha\frac{dg(x,y)}{dx}, \quad \sigma_y(x,y) = Y\alpha\frac{dg(x,y)}{dy}$$

This traction applies everywhere on the thin heated layer, except at the edges. There, the force per unit length F_l applied to the line element defining the boundary of the heated layer is just

$$F_l(x,y) = Y\alpha g(x,y)$$

This force is applied normally to the line element. It can readily be shown for any thin layer of finite dimension that the resultant force on the layer as a whole is zero.

To solve for the flexure of the compensation plate due to the thermoelastic stress of the thin heated layer, we can now simply apply to the plate the opposite of the tractions and line forces required to constrain the thin layer. This problem is easily solved using finite element modeling software such as COMSOL. Finally, the change in the optical path in the recycling cavity is related to the change in thickness of the CP; that is, to the difference in displacement $u_z(x,y)$ of its front and back faces:

$$\Delta z_F(x,y) = (n-1)\left[u_z(x,y)\big|_{back} - u_z(x,y)\big|_{front}\right].$$

10.2 Test mass flexure noise

Since the ring heater acts only upon the barrel of the test mass, the equations describing the surface traction must be modified to account for the inherent curvature of the surface. In the z-direction (along the mirror axis) the surface has no curvature, and the equations for surface traction are basically unchanged. Assuming cylindrical symmetry, within the heated region:

$$\sigma_z(z) = Y\alpha\frac{dg(z)}{dz}$$

and at a line element at the edge of the heated region,

$$F_l(z) = Y\alpha g(z)$$

applied normally to the line element. Here we have generalized the definition of g to a thin layer on the radial boundary of the optic:

$$g(z) = \int T(r,z)dr$$

where $T(r,z)$ is the temperature distribution at the barrel of the optic.

The heated stripe around the barrel of the test mass will expand radially out of the surface by growing thicker. As mentioned earlier, this expansion is unconstrained. The heated stripe will also tend to expand azimuthally by increasing its circumference. This latter expansion will be constrained by a radial stress:

$$\sigma_r(z) = \frac{Y\alpha g(z)}{R}$$

where R is the radius of the test mass. To the extent that the heating is not cylindrically symmetric (that is, $T(r,z) \to T(r,\varphi,z)$) there will also be an azimuthal traction:

$$\sigma_\varphi(\varphi,z) = \frac{Y\alpha}{R}\frac{d\int T(r,\varphi,z)dr}{d\varphi}$$

but we will not consider that possibility here.

10.3 Elasto-optic noise

Once the flexure of the optic is solved in the finite element model, we can apply the elasto-optic coefficients to the strain tensor $\vec{\varepsilon}(x,y,z)$ inside the optic and integrate along the detector beam axis to get the elasto-optic noise profile. Unlike the other noise couplings we consider, this one depends upon the polarization of the interferometer beam. The general form for the elasto-optic coupling is fairly complex, and can be found in Ryan Lawrence's thesis.[3] For the case of the CP, with the IFO light polarization linearly polarized along the y axis,

$$\Delta z_{EO}(x,y) = -\frac{n^3}{2}\int \left\{p_{11}\varepsilon_{xx}(x,y,z) + p_{12}\varepsilon_{yy}(x,y)\right\}dz.$$

10.4 Electrostatic force noise

The ring heater is essentially a wire with a voltage gradient held in proximity to the test mass. Therefore, it will exert an electrostatic force on the test mass. If the voltage is fluctuating, then the electrostatic force too will fluctuate and inject displacement noise into the interferometer.

[3] Ryan Lawrence, Ph.D. thesis, p. 114.

10.4.1 Forces along the beam axis

Figure 10 shows the geometry used in a COMSOL4.1 model used to calculate the electrostatic force coupling along the beam axis.[4] The model is 2d axisymmetric and so assumes that the test mass is a right circular cylinder with no flats, ears, or wedge, and that the ring heater is all at the same potential. We will correct for this latter assumption outside the COMSOL model.

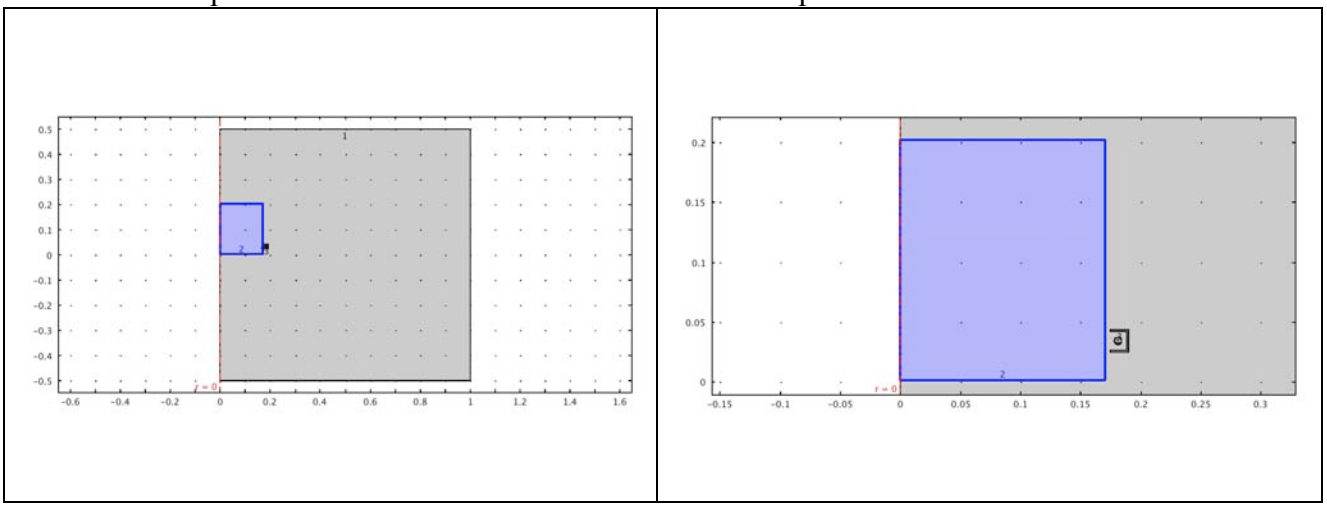

Figure 10: left side; geometry of COMSOL model for electrostatic force calculation, showing test mass, heater, and surrounding ground plane, right side; closeup of test mass and heater.

Rather than use COMSOL4.1's coordinate transformation to produce boundary conditions at infinity, this model uses the fact that the ring heater shield provides a ground plane very close to the heater, and so the fringing fields far from the test mass are ignorably small. It sets the exterior boundary by grounding the outside of the large grey square surrounding the test mass. When the size of this square was doubled, the calculation of the electrostatic force did not change. With 1V on the ring heater, the electric potential distribution is as shown in Figure 11. The electrostatic energy stored in the test mass due to this potential distribution is

$$U = \int \frac{1}{2} \vec{E} \bullet \vec{D} dV ,$$

where $\vec{E}$ is the electric field, $\vec{D}$ is the electric displacement, and the integral is over the volume of the test mass. By varying the position of the test mass along the beam axis within the model and calculating the change in stored dielectric energy we can then obtain the force upon the test mass $F = dU/dx$.[5] For 1V on the heater, the force was found to be $2.5 \times 10^{-13}\ N$.

[4] COMSOL4.1 file 'aLIGO ring heater electrostatic.mph', available from the author.

[5] Strictly speaking, we should calculate the total dielectric energy of the system, both in the test mass and the vacuum around the test mass. This was not possible in the model due to inadequate numerical precision in calculating the energy density in the vacuum. Since the dielectric energy gained by the test mass is at the expense of the energy in the vacuum, which is lower due to the lower permittivity of vacuum compared to glass, the actual change in total energy is less than the change in energy in the test mass. Thus, this calculation overestimates the force and can be taken as a conservative limit.

We now scale this force estimate to account for the actual voltage distribution on the heater. At full power, one segment of the ring heater covering half of the test mass will radiate 5W from a 35Ω load, so its voltage will vary linearly from -6.6V to +6.6V. On top of this static voltage gradient will be a small fluctuating noise voltage δV which also varies linearly across the heater. The electrostatic force is proportional to the voltage squared:

$$F \propto V^2 = (V_0 + \delta V)^2$$

of which the fluctuating part is just $2V_0\delta V = 13.2V \cdot \delta V$. This quantity varies quadratically across the heater, because both V and δV vary linearly, and so the average value of the fluctuating squared voltage over the length of the heater is $1/3 \cdot 2V_0\delta V = 4.4V \cdot \delta V$.

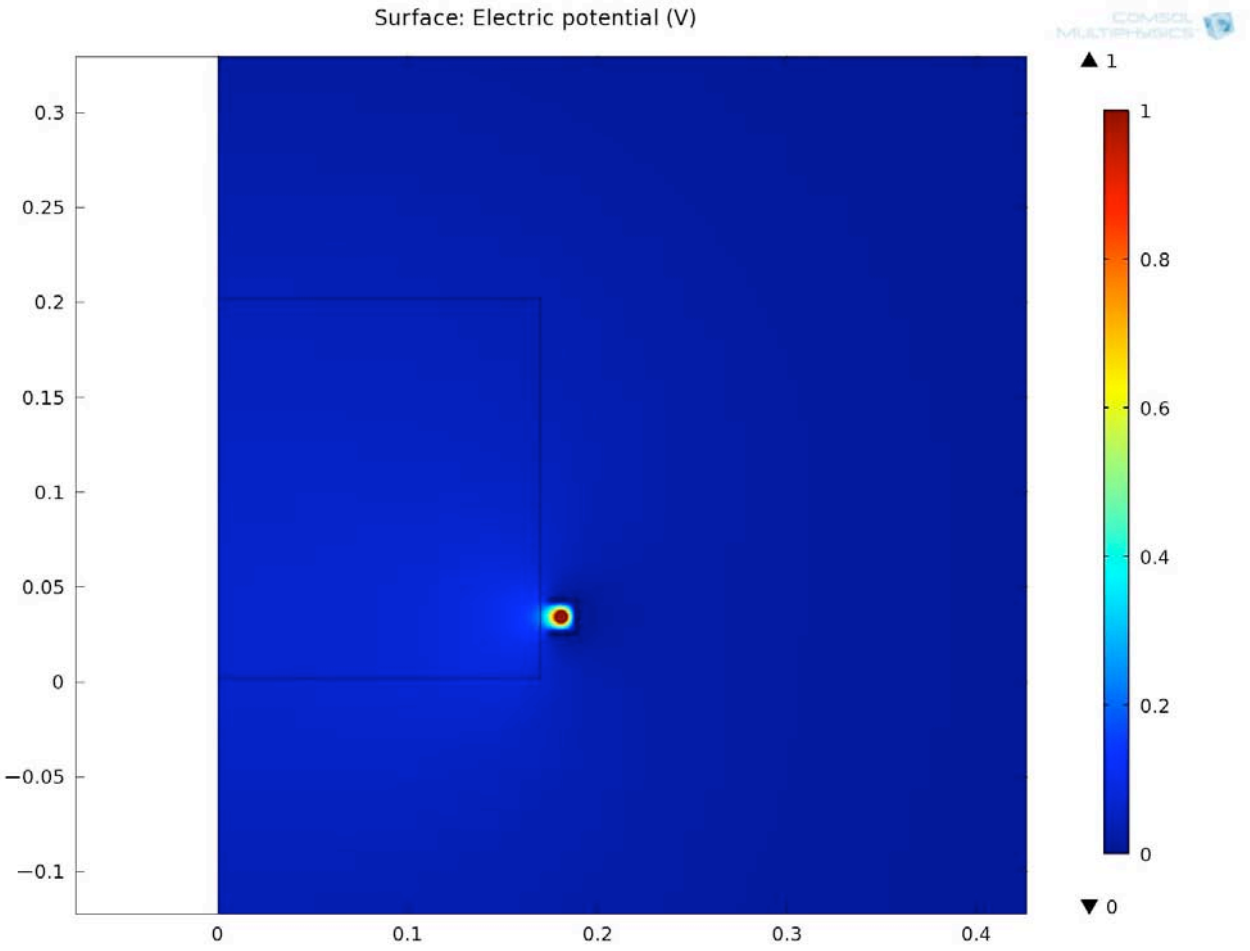

Figure 11: electric potential in and around test mass with 1V on ring heater and shield grounded.

Finally, the fluctuating voltages on the upper and lower ring heater segments will be uncorrelated, which reduces the net force by $\sqrt{2}$. The fluctuating voltage will displace the test mass according to

$$\delta x(f) = \frac{2.5 \times 10^{-13}\ N}{(2\pi f)^2 M} \frac{4.4V \cdot \delta V(f)}{\sqrt{2}(1V)^2}.$$

If we equate this to the technical noise spectrum in Figure 1, then we get the limit on $\delta V(f)$ shown in Figure 12.

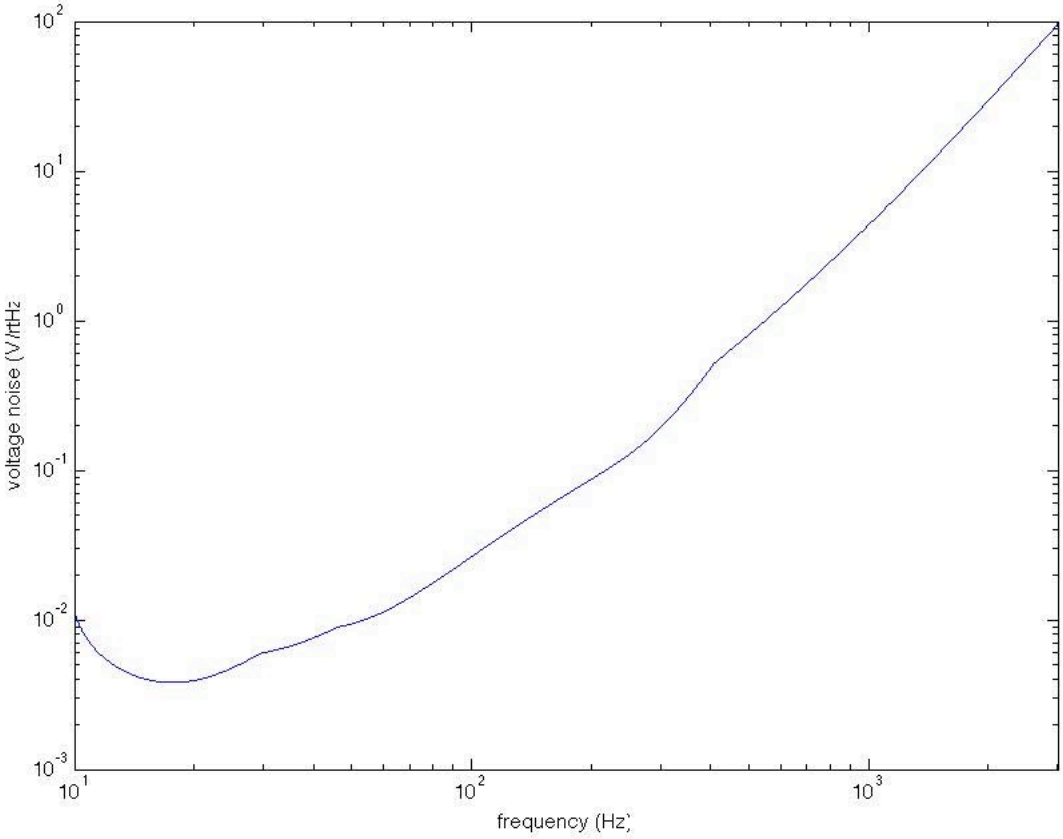

Figure 12: voltage noise requirements for the aLIGO ring heater due to axial electrostatic forces.

As noted before, this voltage noise spectrum is conservative, since the energy variation in the vacuum has not been accounted for. This would be expected to reduce the true force by a factor between 1 and the relative permittivity of glass, or 2.09, and would increase the voltage noise spectrum the same amount.

10.4.2 Forces and torques transverse to the beam axis

As noted above, the voltage fluctuations between the two heater halves are uncorrelated. This raises the possibility of transverse forces and torques. These cannot be modeled axisymmetrically. Figure 13 shows the geometry of a 3D electrostatic model in COMSOL4.1.[6] The test mass remains a right circular cylinder, but a single ring heater segment applies the electrostatic force. The voltage on the ring heater varies linearly from -1V to +1V along the heater.

[6] "aLIGO 3D ring heater electrostatic 2.mph", available from the author.

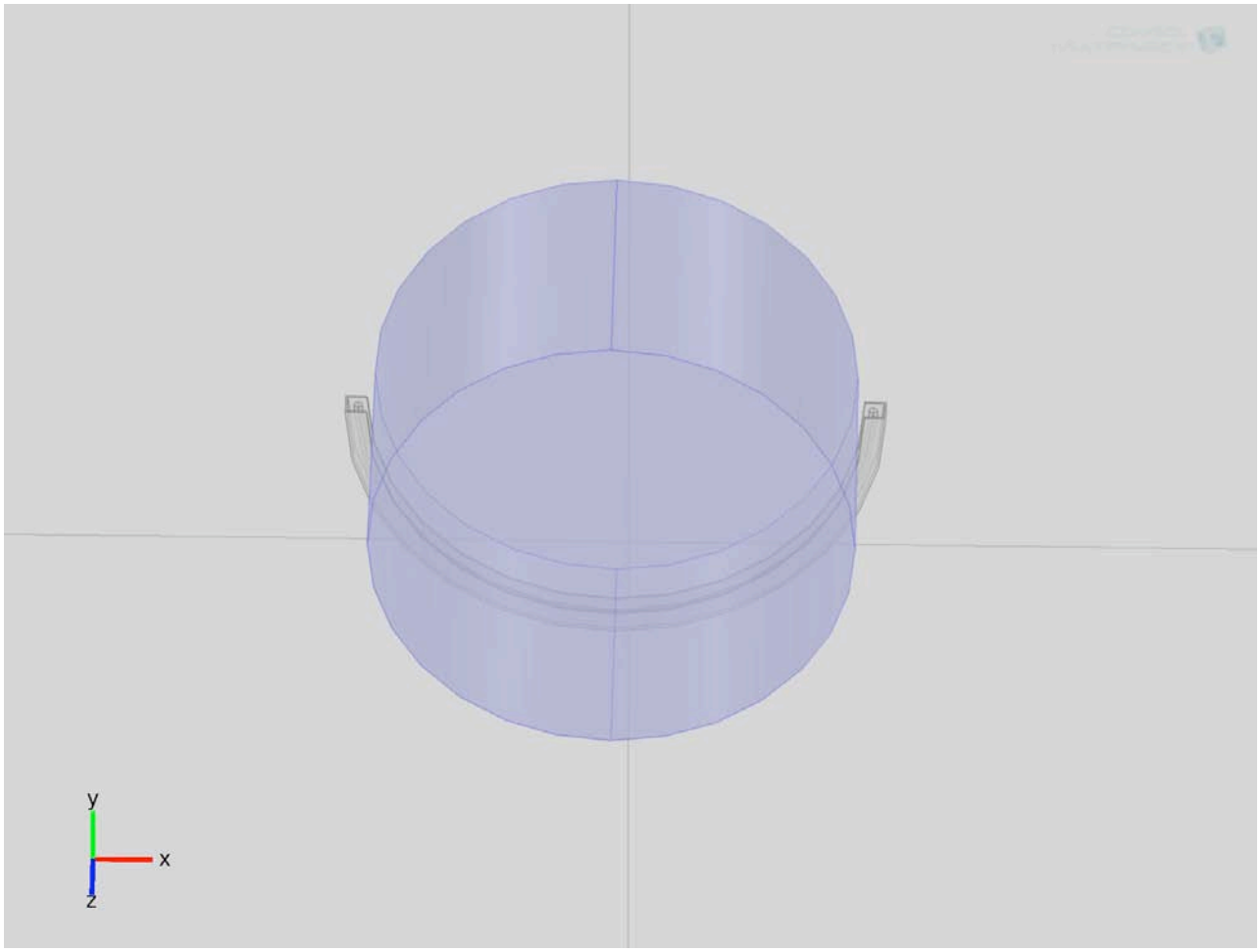

Figure 13: image of test mass and ring heater segment from 3D COMSOL4.1 model. The surrounding ground planes are not shown.

As a test of the consistency between the 2D and 3D models, we also calculated the stored electrostatic energy in a test mass with a full ring heater at uniform 1V potential in the 3D model. The result was $2.04\times10^{-13}\,J$, about 15% less than the 2D model value of $2.37\times10^{-13}\,J$, fair agreement.

Similarly to the 2D model, we moved the test mass toward and away from the ring heater transversely in the y direction and calculated the change in stored energy with position, obtaining a force of $4.0\times10^{-12}\,N$ linear to within ~5% over the 4mm range studied. If we scale this result to the nominal $\pm6.6\,V$ voltage range over the heater, and account for two heater halves with incoherent noise voltages, the transverse displacement noise spectrum is

$$\delta y(f) = \frac{4.0\times10^{-12}\,N}{(2\pi f)^2 40\,kg}\,\frac{2\sqrt{2}(6.6V)\cdot\delta V(f)}{(1V)^2}.$$

If we scale this by 10^{-3} for the cross coupling of y motion to x motion and equate this to the technical displacement noise spectrum in Figure 1, we get the voltage spectrum shown in the left-hand side of Figure 14. This voltage noise requirement is higher than that in Figure 12 by about a factor of 10 and so is less stringent.

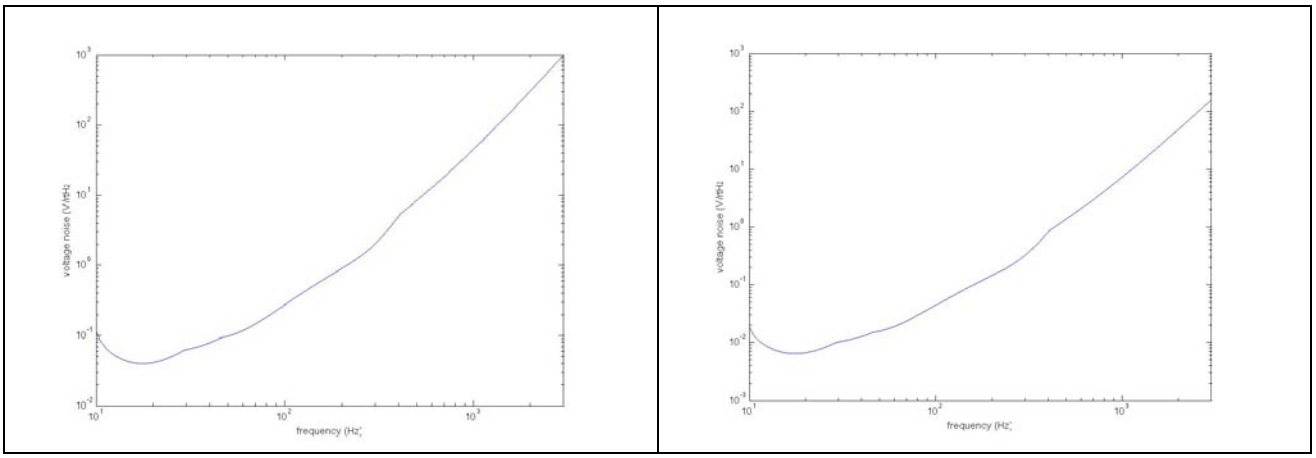

Figure 14: left side, voltage noise requirement due to transverse motion; right side, voltage noise requirement due to torque.

This transverse force is not applied through the test mass center of mass, and so applies a torque. If the interferometer beam is not centered on the test mass, the rotation resulting from this torque will cause an apparent displacement. The test mass moment of inertia around the transverse axis is $0.42\,kg\cdot m^2$, and the ring heater lever arm is 6.57 cm. The rotation of the test mass due to the voltage fluctuations is then

$$\delta\theta(f) = \frac{4.0\times10^{-12}\ N\cdot .0657m}{(2\pi f)^2 0.42kg\cdot m^2}\,\frac{2\sqrt{2}(6.6V)\cdot\delta V(f)}{(1V)^2}$$

and the apparent displacement for 1mm interferometer beam offset[7] is

$$\delta x(f) = \frac{4.0\times10^{-12}\ N\cdot .0657m}{(2\pi f)^2 0.42kg\cdot m^2}\,\frac{2\sqrt{2}(6.6V)\cdot\delta V(f)}{(1V)^2}\cdot 10^{-3}m.$$

Equating this to the technical displacement noise spectrum in Figure 1 yields the voltage noise requirement in the right-hand side of Figure 14. This is a factor of 2 less stringent than the voltage noise spectrum of Figure 12.

11 Appendix: material and interferometer parameters

All parameters are for fused silica unless otherwise noted.

Thermal diffusivity (D_{th})	7.5×10^{-7} m^2/s
Density (ρ)	2202 kg/m^3
Heat capacity (C_v)	739 J/kg/K
Refractive index at 1064 nm (n)	1.45

[7] Taken from T010007-v2.

Refractive index at 10.6 microns	$2.08 + 0.2 \cdot i$
Elasto-optic coefficient (p_{11})	0.121
Elasto-optic coefficient (p_{12})	0.270
Poisson ratio (η)	.167
Arm cavity finesse (F)	445

Thermal expansion coefficient (α)	5.5×10^{-7}/K
Relative permittivity	2.09